Mechanism of crystal-symmetry dependent deformation in ferroelectric ceramics: Experiments versus model

Article *in* Journal of Applied Physics · June 2013

DOI: 10.1063/1.4809979

CITATIONS
8

READS
588

5 authors, including:

Yingwei Li
Peking University
33 PUBLICATIONS **182** CITATIONS
SEE PROFILE

Hongchen Miao
Southwest Jiaotong University
25 PUBLICATIONS **217** CITATIONS
SEE PROFILE

Faxin Li
Peking University
119 PUBLICATIONS **1,040** CITATIONS
SEE PROFILE

AIP | Journal of Applied Physics

Mechanism of crystal-symmetry dependent deformation in ferroelectric ceramics: Experiments versus model

Y. W. Li, X. L. Zhou, H. C. Miao, H. R. Cai, and F. X. Li

Citation: J. Appl. Phys. **113**, 214111 (2013); doi: 10.1063/1.4809979
View online: http://dx.doi.org/10.1063/1.4809979
View Table of Contents: http://jap.aip.org/resource/1/JAPIAU/v113/i21
Published by the AIP Publishing LLC.

JOURNAL OF APPLIED PHYSICS **113**, 214111 (2013)

Mechanism of crystal-symmetry dependent deformation in ferroelectric ceramics: Experiments versus model

Y. W. Li,[1,a)] X. L. Zhou,[1,a)] H. C. Miao,[1] H. R. Cai,[2] and F. X. Li[1,3,b)]
[1]*State Key Laboratory for turbulence and complex systems, College of Engineering, Peking University, Beijing 100871, China*
[2]*Institute of Acoustics, Chinese Academy of Sciences, Beijing 100085, China*
[3]*HEDPS, Center for Applied Physics and Technologies, Peking University, Beijing, China*

(Received 18 March 2013; accepted 27 May 2013; published online 7 June 2013)

In this paper, we investigate the mechanism of crystal-symmetry dependent deformation in ferroelectrics both experimentally and theoretically. We fabricated three types of $Pb(Zr_xTi_{1-x})O3$ ceramics including the tetragonal (PZT45/55), the rhombohedral (PZT60/40), and the morphotropic (PZT52/48), where the tetragonal and rhombohedral phases coexist. X-ray diffraction and piezoresponse force microscopy were performed to characterize the crystal structures and domain patterns. Deformation of both poled and unpoled PZT ceramics was tested under bipolar electric fields and uniaxial compression, respectively. It is found that in both loading cases, the deformation of the morphotropic PZT is obviously larger than that of the tetragonal and rhombohedral PZT. As to the latter two, the electric field induced strain in the tetragonal PZT is smaller than that in the rhombohedral PZT, while the compression induced strains show the opposite tendency. To explore the observed crystal-symmetry deformation mechanism, we employed a previously proposed optimization-based constrained domain-switching model to simulate the experimental results. Domain switching in this model is realized by an optimization process to minimize the free energy of each grain. The constraint from neighboring grains is considered in an Eshelby inclusion manner, which is inherently crystal-symmetry dependent. The simulation results fit well with our experimental results without any fitting parameters, which indicate that the constrained domain-switching is responsible for the crystal-symmetry dependent deformation mechanism in ferroelectric ceramics. © *2013 AIP Publishing LLC*. [http://dx.doi.org/10.1063/1.4809979]

I. INTRODUCTION

Ferroelectric ceramics have been widely used as sensors, actuators, transducers, etc., due to their peculiar electromechanical coupling properties, ultrafast responses, and compact size.[1,2] Among the different ferroelectric ceramics, the lead titanate zirconate (PZT) family of ceramics is the most widely used and has been systematically studied for decades. PZT ceramics show linear piezoelectric behavior under a low electric field/stress, while they exhibit intense nonlinearities when subjected to a high electric field/stress due to domain switching.[3] Domain switching in ferroelectric ceramics is related to the crystal-symmetry. There exists only 180° and 90° domain switching in the tetragonal ferroelectrics, and 180°, 109°, and 71° switching in the rhombohedral ceramics. In ferroelectric single crystals, perfect alignment of polarization can be achieved and a single domain state can exist after being poled by a strong DC field. But the case is quite different in polycrystalline ferroelectrics where the crystallite axes arrange in a random way and multiple domain states could exist after poling. In real ferroelectric ceramics, domain switching is constrained by neighboring domains/grains and may not accomplish completely even under a very large electric field.[2] The level of constraint for domain switching in ferroelectric ceramics is inherently crystal-symmetry dependent as the spontaneous strain of tetragonal PZT ceramics is considerably larger than that of the rhombohedral PZT ceramics.[4–9]

Since the early work by Berlincourt in 1960s,[10] the crystal-symmetry dependent properties of PZT ceramics have been intensively studied including the related domain switching induced nonlinear deformation behavior.[4–7] Hoffmann *et al.*[4] and Kungl *et al.*[5] studied the electric field induced strains in the tetragonal, rhombohedral, and morphotropic PZT ceramics, and they also monitored the structural variations during electric loading using X-ray diffraction. Rogan[6] and Schäufele *et al.*[7] measured the ferroelastic behavior of these three types of PZT ceramics under uni-axial compression. Rogan[6] also observed the microstructure evolution using *in-situ* neutron diffraction. Recently, the crystal-symmetry dependent crack propagation behavior of PZT ceramics was studied by Westram *et al.*[11] So far, it is well known that the tetragonal PZT ceramics are difficult to pole, while the rhombohedral PZT and morphotropic PZT ceramics are easier to Refs. 4 and 5. However, as the related material compositions are somewhat different for different experiments reported in the literature,[4–7,12] complete experimental data under electric and mechanical loading are not available and the related deformation mechanisms are not well studied.

On the other hand, the modeling of domain switching of ferroelectric ceramics has attracted substantial attention in the past decades. For simplicity, most current models consider the

[a)]Y. W. Li and X. L. Zhou contributed equally to this work.
[b)]Author to whom correspondence should be addressed. Electronic mail: lifaxin@pku.edu.

ferroelectric ceramics as tetragonal polycrystallines although in practice the most widely used composition is near the morphotropic phase boundary.[3,13–16] The interactions between domains/grains were either neglected,[3] or taken into account in an Eshelby inclusion manner,[13] or considered using a finite element method.[14] Modeling of the deformation and texture evolution in the rhombohedral PZT ceramics was also conducted and compared with experimental results.[9,17] However, theoretical studies on the crystal-symmetry dependent domain switching in ferroelectrics are quite limited. Li *et al.*[12] studied the lower limit of achievable switching strains in tetragonal, rhombohedral, and morphotropic PZT ceramics through a rigorous mathematical derivation and the Taylor bound estimate. Li and Rajapakse[8,9] proposed an analytical constrained domain switching model for the single-phase tetragonal and rhombohedral ferroelectric ceramics, taking the interactions between grains using the Eshelby inclusion method. Later, this analytical model was developed to a computational model in which domain switching is realized by an optimization process.[18–20] Tang *et al.*[21] also considered the interaction between grains in an inclusion manner and studied the domain switching in three types of PZT ceramics using the Monte-Carlo method. Despite this progress, the crystal-symmetry dependent domain switching mechanism is still not well understood because the above-mentioned studies are either purely theoretical[8,9,12,18–20] or used fitting parameters to capture the experimental results.[21]

In present study, in order to explore the mechanism of crystal-symmetry dependent deformation in ferroelectric ceramics, we first fabricated three types of PZT ceramics including the tetragonal (PZT45/55), the rhombohedral (PZT60/40), and the morphotropic (PZT52/48) where tetragonal and rhombohedral phases coexist. Deformation of both poled and unpoled PZT ceramics was then tested under applied bipolar electric fields and uniaxial compression, respectively. To simulate the experimental results, we employed our previously proposed constrained domain switching model for polycrystalline ferroelectrics in which the domain switching is realized by an optimization process to minimize the free energy of each grain. The measured material properties were taken as input to the model and no fitting parameters were used. The simulation results on the tetragonal, rhombohedral, and morphotropic PZT ceramics fit well with our experimental results without any fitting parameters, confirming that the constrained domain-switching is responsible for the crystal-symmetry dependent deformation mechanism in ferroelectric ceramics.

II. EXPERIMENTAL PROCEDURE

A. Material fabrication and sample preparation

In this work, we first fabricated three types of $Pb(Zr_xTi_{1-x})O_3$ ceramics using the conventional mixed oxide method with the Zr/Ti ratio at 45/55 (tetragonal), 52/48 (morphotropic), and 60/40 (rhombohedral), respectively. A small amount of La doping was used for all compositions to make the PZT ceramics soft. The stoichiometric PbO, ZrO2, and TiO2 powders were mixed and wet-milled for 24 h using ZrO2 balls and alcohol as the milling media. The slurries were dried at 250° C and then sieved with a mesh of size 0.5 mm. The sieved powder was pre-sintered at 800 °C for 1 h and then sieved again with a mesh of size 0.13 mm. The bar-shaped green compacts for mechanical loading and the penny-shaped green compacts for electrical measurements were both formed by dry pressing at 100 MPa and 70 MPa, respectively. The green compacts were then placed in an alumina crucible and sintered at 1300° C in a PbO atmosphere with the holding time of 2 h. The heating rate was controlled at 3° C per min and the cooling process in the furnace lasted for about 4 h.

The sintered bar-shaped bodies were cut to $6 \times 6 \times 12\,mm^3$ specimens for compression testing. For electrical measurements, silver paste was spread on the two $6 \times 6\ mm^2$ faces of the bar-shaped specimens as well as both faces of the penny-shaped discs and then sintered at 700° C for 10 min. Electric poling was accomplished at 330° C by a DC field of 500 V/mm along the 12 mm direction with the holding time of 30 min. The temperature was gradually cooled to room temperature with the electric field holding. After poling, the d_{33} constants were measured using a Berlincourt d_{33} meter. The average d_{33} value is 495pC/N for the morphotropic PZT, 180pC/N for the rhombohedral PZT, and 140pC/N for the tetragonal PZT, respectively.

B. Structural characterization

The crystal structures of the three types of PZT were characterized by X-ray diffraction using Cu$K\alpha$ radiation (Rigaku, Tokyo, Japan), with the wavelength of $\lambda_\alpha = 1.54046$ Å and $\lambda_\beta = 1.54439$ Å. Its 2θ angle resolution is 0.001°. The lattice constants as well as the volume fractions of the tetragonal phase and rhombohedral phase in the morphotropic (PZT 52/48) ceramics were determined by the Rietveld refinement. The lattice constants are then used to calculate the spontaneous strains in each type of PZT ceramics.[2,8,9]

The domain patterns of these PZT ceramics were characterized by piezoresponse force microscopy (PFM) using a MFP-3D atomic force microscope (Asylum Research, CA, US). The wafer shaped samples for PFM testing were carefully polished until the surface roughness was less than 20 nm. To enhance the signal to noise ratio (SNR) of the piezoelectric response, a dual-frequency resonance-tracking (DFRT) technique was used to drive the sample-cantilever system near the contact resonance frequency.[22]

C. Macroscopic deformation testing

The deformation behavior of the three types of unpoled PZT ceramics under bipolar electric loading was tested using penny shaped samples with the thickness of 2 mm. The testing setup is shown in Fig. 1(a). The polarization variations during electric loading were measured by a ferroelectric analyzer (Radiant LC) using an external power supply with the maximum applied voltage of 10 kV. The strain of the wafer shaped specimen along the thickness direction was measured using a high resolution LVDT (Macro Sensors, NJ, US) with

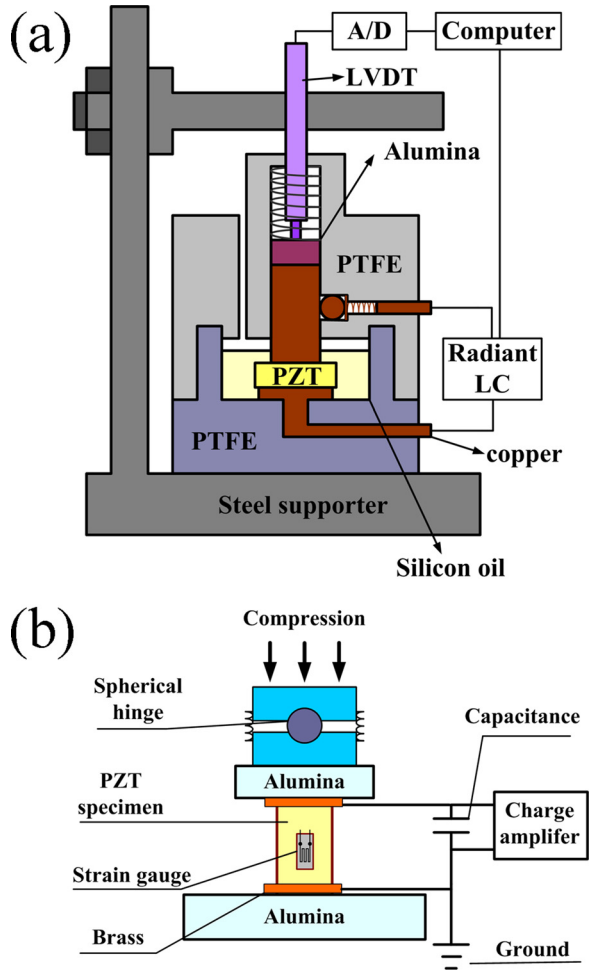

FIG. 1. Experiment setups for (a) D-E hysteresis loop and butterfly curve measurement and (b) stress-strain curve and stress-depolarization curve measurement.

the accuracy better than 0.15 μm. The specimen was immersed into an insulation tank filled with silicon oil to prevent charge leakage and arcing. To make the strain signals more stable during testing, the LVDT was tightly pressed to the alumina plate and the copper cylinder on the top electrode of the PZT specimen. The period for the electric loading was set to 5 s to make the domain switching process quasi-static and comparable to that under compression loading.

The deformation behavior of both the unpoled and poled PZT ceramics under uni-axial compression was then tested using the $6 \times 6 \times 12$ mm^3 bar-shaped specimens. The testing setup for uni-axial compression loading is shown in Fig. 1(b), where the compression is provided by a screw-driven testing machine (Shimadzu, Japan). A spherical hinge was used to avoid bias compression. During compression, the longitudinal strains were measured using strain gauges bonded on the two opposite 6×12 mm^2 faces and the polarization variations of the poled specimens were measured by a high-resistance charge amplifier. To realize the quasi-static deformation, the compression loading rate was set to 5 MPa/s and the unloading rate to about 10 MPa/s. The signals of the applied force, strains and polarizations were acquired simultaneously by a 16-bit A/D card and monitored by a computer.

III. EXPERIMENTAL RESULTS AND DISCUSSIONS

A. X-ray diffraction

Fig. 2 shows the powder X-ray diffraction results of the PZT 45/55, PZT52/48 and PZT 60/40 ceramics. It can be seen that the 200 and 002 double peaks turn to a 002 single peak around $2\theta = 44°$ when the Zr/Ti ratio increases from 45/55 to 60/40, indicating that the material structure changes from tetragonal to rhombohedral. According to the Laue equation, the lattice constants of the tetragonal phase can be calculated using $a = b = 2 \cdot d^T_{200} = \lambda/\sin\theta^T_{200}$ and $c = 2 \cdot d^T_{002} = \lambda/\sin\theta^T_{002}$ and that of the rhombohedral phase can be calculated by $\alpha = 2 \cdot \arctan((\sqrt{3}d^R_{001})/(2d^R_{111}))$ and $a = b = c = \sqrt{(d^R_{111})^2/\left(1 - \sin^2(\alpha/2) \cdot 4/3\right)}$, where d^R_{001} and d^R_{111} are equal to $\lambda/(2\sin\theta^R_{001})$ and $\lambda/(2\sin\theta^R_{111})$, respectively. In the morphotropic PZT, the intensity peaks of the tetragonal phase and the rhombohedral phase overlap with each other and cannot be distinguished accurately. The Rietveld refinement method was then employed to obtain their lattice constants and volume fractions.[23] No attempts were made to verify the presence of the possible monoclinic phase.[24] The single crystal deformation of the tetragonal phase and the rhombohedral phase were calculated by using $S^T_0 = S^T_{lattice} = \frac{c}{a} - 1$ and $S^R_0 = \frac{9}{8}S^R_{lattice} = \frac{9}{8}(\frac{d^R_{111}}{d^R_{-111}} - 1)$,[2,8,9,25] respectively.

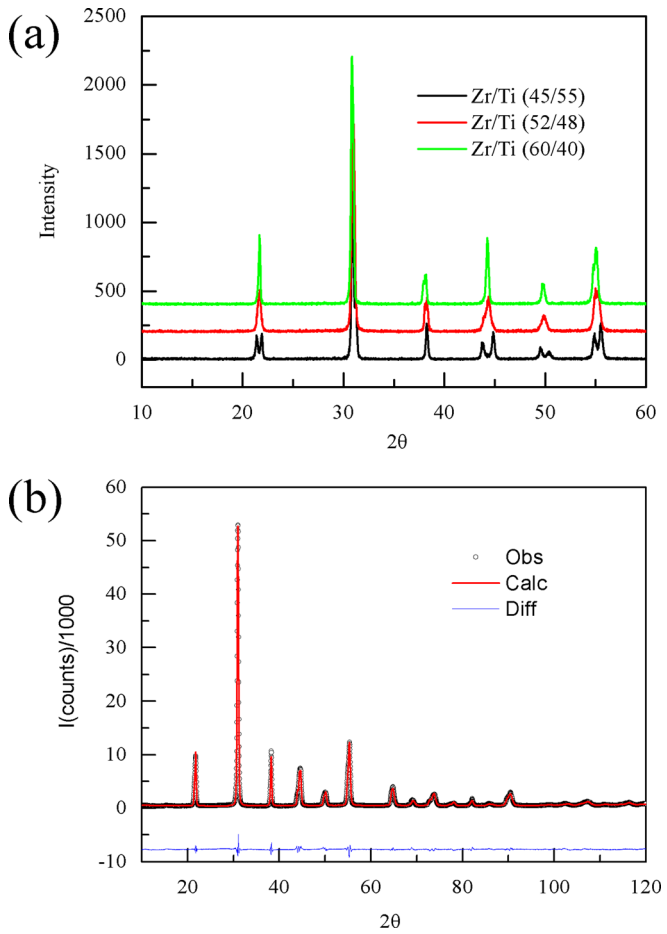

FIG. 2. (a) Powder X-ray diffraction results of the PZT 45/55, PZT52/48, and PZT 60/40, (b) observed and calculated diffraction profiles from the Rietveld refinement of the morphotropic PZT (52/48). The difference plots are shown.

TABLE I. Lattice constants and single-crystal deformations of three types of PZT ceramics determined by X-ray diffraction.

Zr/Ti ratio	Crystal symmetry	Lattice constant		Single crystal deformation S_0 (%)
45/55	Tetragonal	a = b = 4.041 Å	c = 4.1358 Å	2.35
60/40	Rhombohedral	a = 4.0958 Å	$\alpha = 89.7367°$	0.69
52/48	Tetragonal (52%)	a=b = 4.0506 Å	c = 4.1090 Å	1.44
	Rhombohedral (48%)	a = 4.0648Å	$\alpha = 89.5393°$	1.2

Both the lattice constants and the single crystal deformations for these three types of PZT are listed in Table I.

B. Piezoresponse force microscopy

Fig. 3 shows the PFM images of the three types of PZT ceramics. It can be seen from Fig. 3(a) that in tetragonal PZT ceramics, the stripe-like domain patterns can be clearly observed in both the PFM amplitude image and phase image. The stripe-like domains are 90° domains based on the strain compatible conditions in tetragonal ferroelectrics and the domain width is estimated to be about 80 nm. The 180° domain walls can be clearly seen from the phase image which accords with the amplitude image very well. However, in the rhombohedral and morphotropic PZT ceramics, only the 180° domain patterns can be seen and the non-180° domains are difficult to distinguish probably because the non-180° domain wall densities in these two PZT ceramics are not as high as that in the tetragonal PZT ceramics.[4]

C. Electric loading

Fig. 4 shows the measured D-E hysteresis loops and butterfly curves of the tetragonal, rhombohedral, and morphotropic PZT ceramics during bipolar electric loading. It can be seen that all the three types of PZT ceramics can be fully poled under the maximum applied electric field (4 kV/mm for the tetragonal and rhombohedral PZT, 3 kV/mm for the morphotropic PZT as a field higher than 3 kV/mm is apt to make electric breakdown of the sample). The coercive field of the tetragonal PZT ceramics (about 2.5 kV/mm) is significantly larger than that of the rhombohedral and morphotropic PZT (both are about 1 kV/mm). As to the maximum field-induced polarization and strain, the morphotropic PZT ceramics is the largest, the tetragonal PZT the smallest, and the rhombohedral PZT is modest, which are consistent with previous observations[4,5] but of slightly different values. The remnant polarization and strain follows the same trend and are equal to 42 μC/cm^2, 38 μC/cm^2, 30 μC/cm^2 and 0.38%, 0.19%, and 0.12% for the morphotropic, rhombohedral, and tetragonal PZT ceramics, respectively. This behavior can be well explained by previous models[8,9,18–20] because the Taylor bound strain is non-zero in the morphotropic PZT ceramics but zero in both the tetragonal and rhombohedral ceramics. However, a quantitative comparison between experiments and simulations is not yet available.

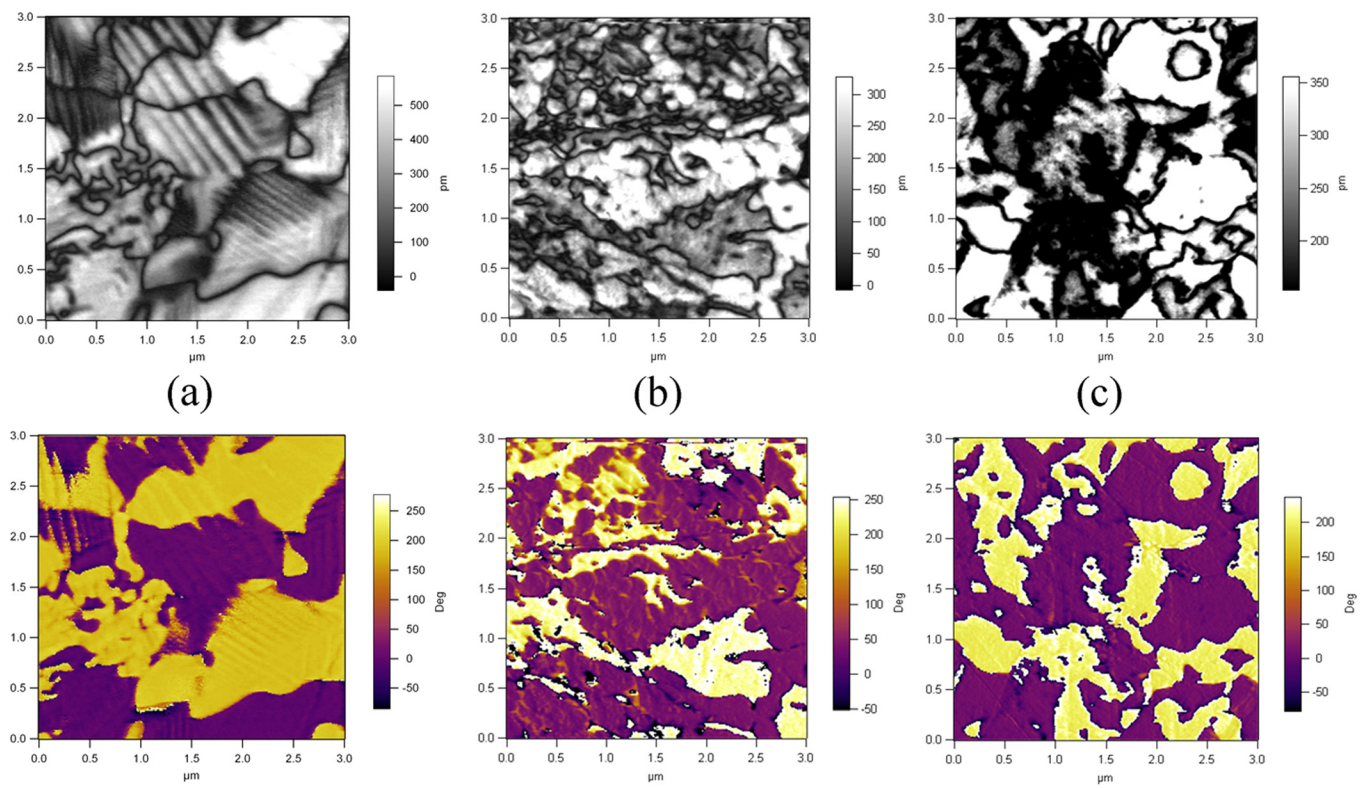

FIG. 3. The PFM amplitude images (up) and phase images (below) of the three types of PZT ceramics. (a) Tetragonal; (b) rhombohedral; (c) morphotropic.

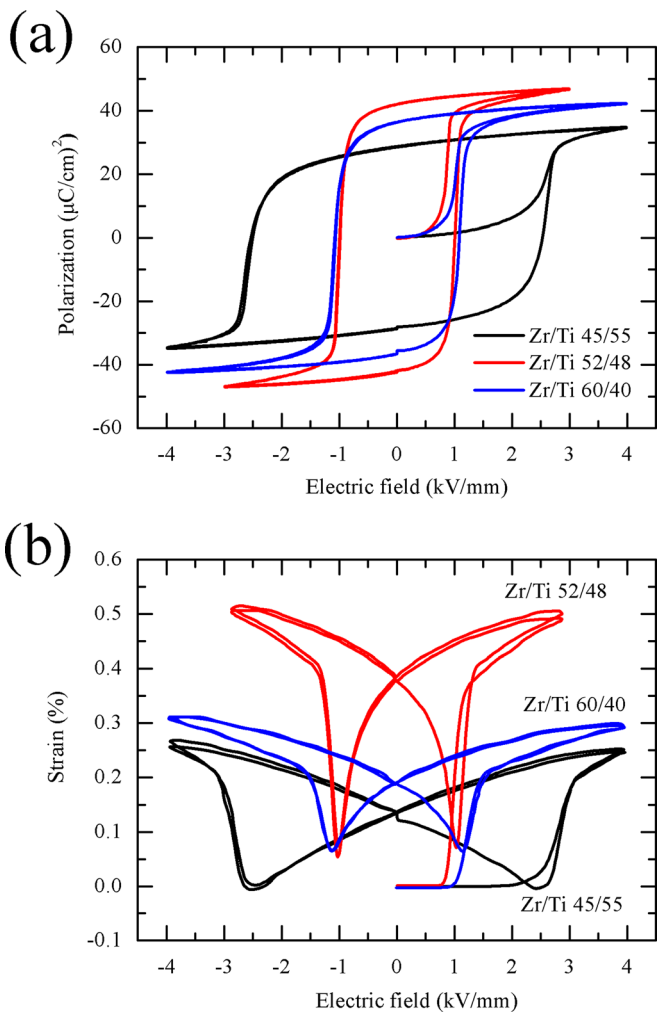

FIG. 4. The measured D-E hysteresis loops and butterfly curves of the tetragonal, rhombohedral and morphotropic PZT ceramics during electric poling.

D. Mechanical loading

Fig. 5 shows the stress-strain curves of the three types of unpoled PZT ceramics during uni-axial compression loading/unloading with the maximum stress of 400 MPa. It can be seen that the ferroelastic domain-switching induced nonlinearity occurs at a much lower stress in the morphotropic PZT ceramics than that in the tetragonal and rhombohedral PZT ceramics, and for all the samples, the coercive stress is not distinct. With regard to the maximum stress-induced strains, the morphotropic PZT is the largest, the rhombohedral PZT is the smallest, and the tetragonal is in between. This is different from previous experiments[6] where the stress induced strain in the rhombohedral PZT ceramics is larger than that in the tetragonal PZT. This may be due to the fact that in Ref. 6, the composition for the tetragonal phase is PZT40/60 which has a larger tetragonality (c/a = 1.0336) or lattice strain (c/a-1 = 3.36%), while in this work, the tetragonal composition is PZT 45/55, which has a relatively smaller tetragonality (c/a = 1.0235). In PZT ceramics with a smaller lattice strain, the ferroelastic domain switching is less constrained and more domains can switch under a large electric field or a high stress.[8,9] Thus, the tetragonal PZT ceramics in

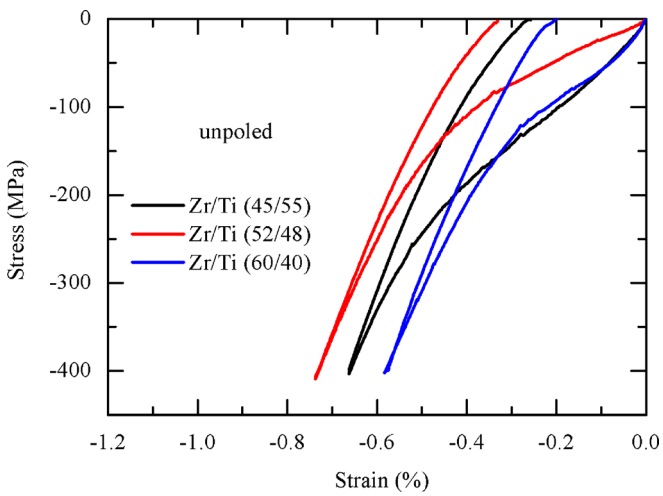

FIG. 5. The measured stress-strain curves of the three types of unpoled PZT ceramics.

this work may have a larger deformation than that in Ref. 6. The resisting field/stress (or back field/stress) generated by ferroelastic domain switching is proportional to the square of the lattice strain during electric loading but only proportional to the lattice strain during stress loading.[8] The switching induced strain is the product of the lattice strain multiplied by the volume fraction of ferroelastic switching, thus it is acceptable that the compression induced strains of the tetragonal and rhombohedral PZT in Fig. 5 do not follow the same trend as the electric field induced strains in Fig. 4(b).

Fig. 6 shows the measured stress-strain curves and stress-depolarization curves of the three types of poled PZT ceramics during mechanical depolarization. It can be seen that as expected the morphotropic PZT shows the largest remnant strain and polarization. For the tetragonal and rhombohedral PZT, the remnant strains are very close to each other. However, the remnant polarization of the rhombohedral PZT is considerably larger than that of the tetragonal PZT, which may indicate that after electric poling, reverse domain-switching occurs in the tetragonal PZT. The coercive stress at which the nonlinearities occur shows the same tendency in both the stress-strain curves and stress-depolarization curves, i.e., it is smallest in the morphotropic PZT, largest in the tetragonal PZT and in the middle for the rhombohedral PZT.

For a complete comparison, the remnant strains and polarizations after electric poling and compression loading in Figs. 4–6 have been measured and listed in Table II. Theoretically, if domain switching under electric poling and compression loading were both saturated and no reverse domain switching occurs upon removal of the field/stress, then we have the following relations:

$$S_E^r + S_\sigma^r = S_{DP}^r, \tag{1}$$

$$P_E^r > P_{DP}^r, \tag{2}$$

where S_E^r, S_σ^r, are the remnant strains of the unpoled PZT ceramics after electric poling and compression loading, respectively; S_{DP}^r is the remnant strain of poled PZT ceramics after compression depolarization; P_E^r and P_{DP}^r are

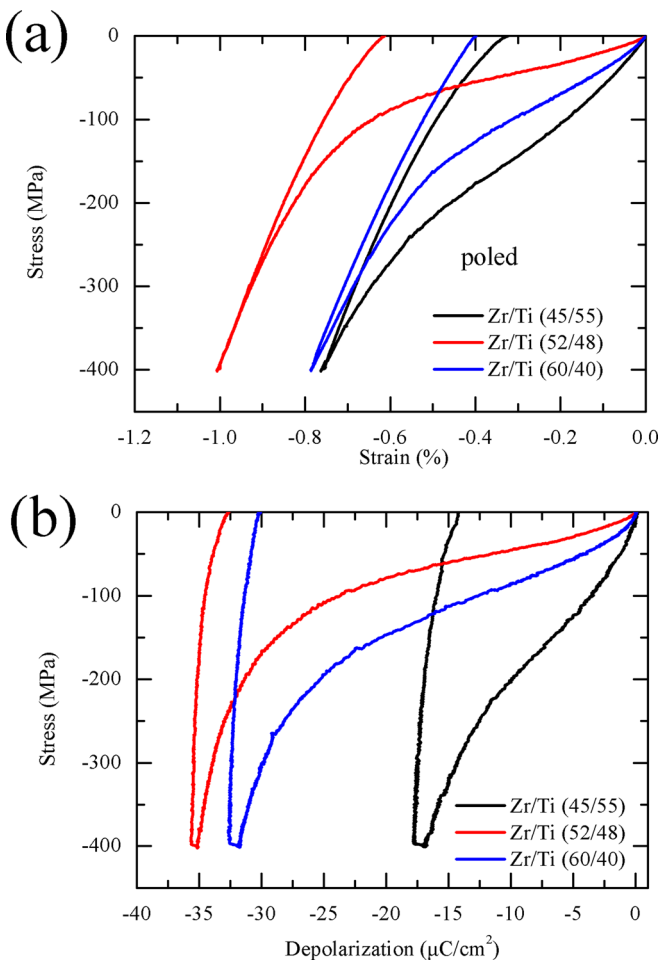

FIG. 6. The measured (a) stress-strain curves and (b) stress-depolarization curves of the three types of poled PZT ceramics.

the remnant polarizations of unpoled PZT after electric poling and that of poled PZT after compression depolarization, respectively.

Equation (1) is easy to understand and it implies that the saturated ferroelastic domain states for both unpoled PZT and poled PZT after compression loading are the same, and no reverse ferroelastic domain switching occurs after electric poling. The inequality (2) indicates that the remnant polarization of a poled ferroelectric ceramic cannot be fully removed by a compression loading and the more accurate expression of (2) is $P^r_{DP} = 0.79P^r_E$ for tetragonal ceramics and $P^r_{DP} = 0.83P^r_E$ for rhombohedral ceramics (Where $P^r_E = 0.83P_0$ for tetragonal ceramics and $P^r_E = 0.87P_0$ for rhombohedral ceramics, P_0 represents the spontaneous polarization).[26,27] For the morphotropic ceramics, the analytical relation between P^r_{DP} and P^r_E is not available, but they should be more close to each other than that in the tetragonal and rhombohedral ferroelectric ceramics.

From Table II, it can be seen that inequality (2) is satisfied for all the three types of PZT ceramics although the more accurate expression cannot be satisfied. However, Eq. (1) is nearly satisfied only for the rhombohedral PZT. For the tetragonal and morphotropic PZT, it appears that

$$S^r_E + S^r_\sigma > S^r_{DP}. \tag{3}$$

The reason for inequality (3) should be due to the fact that after poling usually partial reverse ferroelastic domain-switching occurs upon removing the poling field. However, if so, inequality (3) should also apply for the rhombohedral PZT but actually it does not. We think that in the rhombohedral PZT, during high temperature poling with the holding time of 30 min, the maximum strain is larger than that during room-temperature poling in Fig. 4(b), and upon removing the poling field after cooling, the remnant strain can still be kept no less than 0.19% although some reverse switching occurs. Such effect should also appear in the tetragonal PZT, but the large lattice deformation may make the reverse ferroelastic switching more severe after poling. As to the morphotropic PZT, because the electric field induced strain is almost saturated during room-temperature poling, it cannot be increased any more even under high temperature poling.

Taking into account the lattice deformation measurements in Table I and the theoretically saturated strains in ferroelectric polycrystalline under electric loading and compression loading,[27] it can be deduced that the saturated remnant strains after electric poling and compression loading are 0.368 $S^T_0 = 0.86\%$ and $0.269S^T_0 = 0.63\%$ for the tetragonal PZT, $0.424S^R_0 = 0.29\%$ and $0.286S^R_0 = 0.20\%$ for the rhombohedral PZT, respectively. For the morphotropic PZT, only the theoretically saturated strain after electric poling is available, which is $0.217S^T_0 + 0.309S^R_0 = 0.69\%$. A comparison of the theoretically saturated strains with the corresponding measured values in Table II shows that for both electric loading and mechanical loading, the domain-switching induced strains in the rhombohedral PZT is closer to the saturated values than the tetragonal PZT. Furthermore, for both tetragonal and rhombohedral PZT ceramics, the switching strains under mechanical loading are closer to the saturated values than that under electric loading, which is consistent with the previous observations for soft PZT ceramics.[28]

IV. THE OPTIMIZATION-BASED CONSTRAINED DOMAIN SWITCHING MODEL

To explore the mechanism of the observed crystal-symmetry dependent deformations in PZT ceramics, we employed our previously proposed optimization-based constrained domain switching model to simulate the experimental results.[18,20] In this model, a polycrystalline ferroelectric ceramics is assumed to compose of numerous randomly oriented grains, each containing N types of domains (N = 6 for the tetragonal, N = 8 for the rhombohedral, and N = 14 for the morphotropic ceramics). For the morphotropic ceramics, the field induced phase transformations between the tetragonal phase and rhombohedral phase are permissible thus both the in-phase and inter-phase domain-switching can occur in this model. Charge screening effect in real ferroelectric ceramics[29,30] is taken into account in the model. That is, the depolarization field induced by polarization gradient or polarization switching is completely compensated by free charges. The internal stress field caused by the spontaneous strain change during non-180° domain switching, however, cannot be compensated in a similar way and is considered in an Eshelby inclusion manner[31] Domain switching

TABLE II. Remnant strains and polarizations of three types of PZT ceramics after electric poling and compression loading. Strains in the brackets are the theoretical saturated values calculated using the lattice constants.

	Unpoled PZT after electric poling		Unpoled PZT after compression	Poled PZT after compression depolarization	
Remnant strain (%) and polarization (μC/cm^2)	Strain (S_E^r)	Polarization (P_E^r)	Strain (S_σ^r)	Strain (S_{DP}^r)	Polarization (P_{DP}^r)
Tetragonal	0.12 [0.86]	30	0.26 [0.63]	0.33	14
Rhombohedral	0.19 [0.29]	38	0.20 [0.20]	0.4	30
Morphotropic	0.38 [0.69]	42	0.33	0.62	33

is realized automatically via an optimization process[32] to minimize the free energy of each grain using the volume fractions of domains as the optimization variables, which is very similar to the manner used in phase field models.[15,33–36]

Under a prescribed electromechanical loading, the free energy of a specific grain is expressed as

$$\begin{aligned} U(\mathbf{E},\boldsymbol{\sigma}) = & -\mathbf{E}\cdot\mathbf{P}^r - \boldsymbol{\sigma}:\boldsymbol{\varepsilon}^r + \frac{1}{2}k\mathbf{E}\cdot\mathbf{E} \\ & + \frac{1}{2}\frac{1}{2\mu}\boldsymbol{\sigma}:\boldsymbol{\sigma} - \frac{1}{2}\frac{v}{2\mu(1+v)}[tr(\boldsymbol{\sigma})]^2 \\ & + \frac{1}{2}\cdot 2\mu\frac{7-5v}{15(1-v)}(\boldsymbol{\varepsilon}^r - \bar{\boldsymbol{\varepsilon}}):(\boldsymbol{\varepsilon}^r - \bar{\boldsymbol{\varepsilon}}) \\ & + f_{180}\cdot W_{180} + f_{non-180}\cdot W_{non-180}, \end{aligned} \quad (4)$$

where $\mathbf{E}$,$\boldsymbol{\sigma}$ are the applied electric field vector and applied stress tensor, respectively; k is the isotropic dielectric constant; μ, v are the isotropic shear modulus and poisson ratio; $\bar{\boldsymbol{\varepsilon}}$ is the mean strain tensor of the whole material system or the matrix; and $\mathbf{P}^r$ and $\boldsymbol{\varepsilon}^r$ are the remnant polarization vector and remnant strain tensor of a grain which can be expressed as linear functions of the volume fractions of domains. Details of this constrained domain switching model can be found elsewhere[18,20] and will not be reiterated here.

V. SIMULATION RESULTS AND DISCUSSION

We then use the proposed constrained domain switching model to investigate the crystal-symmetry dependent deformation and polarization in PZT ceramics. To make the model more predictive and to explore the intrinsic deformation mechanism, no fitting parameters are used in the model. The energy barriers for both the 180° and non-180° domain switching (also including the interphase domain switching in morphotropic PZT) are taken to be $2P_0E_C$ (where P_0 is the single-crystal spontaneous polarization and E_C the coercive field). For all types of PZT ceramics, the single-crystal spontaneous polarization P_0 is taken as 0.52 C/m^2 (Ref. 10) and the Poisson ratio v is 0.3. Other parameters required in the simulations including the coercive field E_C, the single crystal deformation S_0, the isotropic shear modulus μ, etc., are taken from the X-ray diffraction data and the measured strain/polarization curves under electric/stress loading given in Figs. 4–6. All parameters used in the simulation are listed in Table III.

We first conducted simulations of domain switching in the three types of unpoled PZT ceramics subjected to cyclic electric loading and compression loading/unloading. Then, all the unpoled PZT ceramics were poled by a large unipolar electric field, the field was gradually removed and thereafter the specimens were subjected to uni-axial compression depolarization.

Fig. 7 shows the simulated D-E hysteresis loops and butterfly curves of the tetragonal PZT, the rhombohedral PZT and the morphotropic PZT ceramics during cyclic electric loading. It can be seen that for both the remnant polarization and remnant strains under electric loading, the morphotropic PZT gives the highest values followed by the rhombohedral PZT and the tetragonal has the smallest values. This is consistent with the experimental observations in Fig. 4. The corresponding values from the simulations are also very close to the experimental results except that for the remnant strains, the simulated value is slightly larger than the measured value for tetragonal PZT, while it is lower for the morphotropic PZT. As to the shapes of the polarization and strain curves, the slopes of the simulated D-E hysteresis curves near the coercive field are always smaller than that in the measured curves, and the simulated butterfly curves do not have the long tails as observed in the morphotropic PZT in Fig. 4(b). This may be due to the fact that in the simulations, both the

TABLE III. Material constants of three types of PZT ceramics used in the simulations.

	Single phase PZT		Morphotropic PZT	
Material constants	Tetragonal	Rhombohedral	Tetragonal	Rhombohedral
Shear modulus μ(GPa)	20	20	10	
Poisson ratio v	0.3			
Dielectric constant k (F/m)	1.2×10^{-8}	1.2×10^{-8}	1.4×10^{-8}	
Spontaneous polarization P_0 (C/m^2)	0.52			
Single crystal deformation S_0 (%)	2.35	0.69	1.44	1.2
Coercive field E_C (kV/mm)	2.0	1.0	1.0	

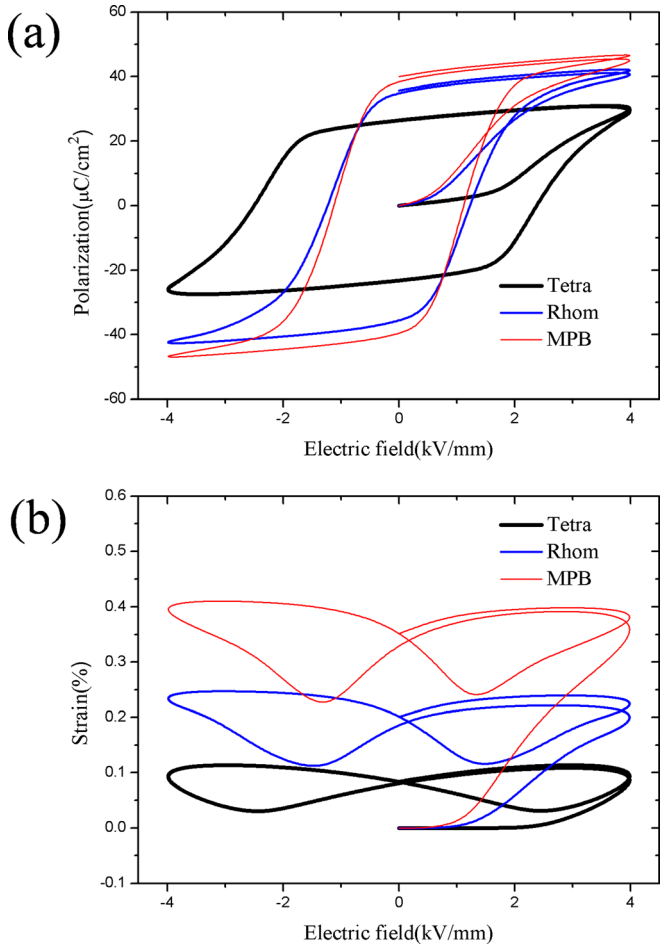

FIG. 7. The simulated D-E hysteresis loops and butterfly curves of the tetragonal, rhombohedral and morphotropic PZT ceramics during electric loading.

loading and domain switching are quasi-static processes and the obtained states are always in equilibrium. While in the experiments, domain switching is a dynamic process which makes the loading process also dynamic, thus the measured states near the coercive field are always in non-equilibrium. Taking this observation into account, hereafter in this paper, we only compare the equilibrium states, i.e., the saturated states and remnant states between the simulations and the experimental results.

A comparison of the simulated strains in Fig. 7(b) and the measured strains in Fig. 4(b) shows that the simulated maximum strain is always smaller than the measured maximum strain in all three types of PZT ceramics. This is due to the fact that in a real ferroelectric ceramic, the internal stresses caused by ferroelastic domain switching cannot be that large because the defects such as grain boundaries, dislocations, etc., may partially release the internal stresses. Furthermore, in experiments, domain switching may occur simultaneously in many grains, while in the simulations it can only occur in one grain at each calculation step. The latter also tends to overestimate the internal stresses caused by ferroelastic domain switching and underestimate the switchable strains, especially when the lattice deformation is large, such as in the case of tetragonal PZT. In addition, it can also be seen that upon removing the poling field, the measured

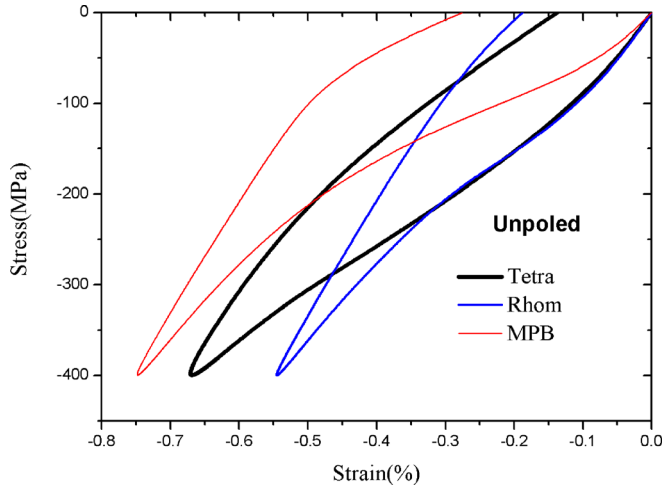

FIG. 8. The simulated stress-strain curves of three types of unpoled PZT ceramics.

strains decrease more quickly than the simulated strains especially in the morphotropic PZT ceramics, indicating that the reverse ferroelastic domain switching is more significant in experiments which is assumed to be caused by the internal bias field in real ferroelectric ceramics.[37] This effect is not included in the proposed model, thus the model is apt to underestimate the volume fractions of reverse domain switching after electric poling.

Fig. 8 shows the simulated stress-strain curves of the three types of unpoled PZT ceramics. It can be seen that both the maximum strain and remnant strain of the morphotropic PZT is the largest among the three, and the maximum strain of the tetragonal PZT is larger than that of the rhombohedral PZT. This behavior fits well with the experimental observations in Fig. 5. However, the simulated remnant strain of the tetragonal PZT is smaller than that of the rhombohedral PZT, which is just opposite to the experimental results. It can also be seen that in Fig. 8, significant reverse ferroelastic switching occurs in the tetragonal PZT and the morphotropic PZT upon removing the compressive stress, while the reverse domain-switching is not so obvious in the rhombohedral PZT. This is due to the fact that both the tetragonal PZT and rhombohedral PZT ceramics have less than five independent deformation modes which make them theoretically brittle according to the Taylor rule of plasticity.[38] The tetragonal PZT ceramics has a much larger single-crystal-deformation of 2.35% compared to that of only 0.69% in the case of rhombohedral PZT. Thus, during ferroelastic domain switching much larger internal stresses are generated in the tetragonal PZT because of the elastic Eshelby inclusion assumption in the model, which is apt to cause significant reverse domain switching upon removing the compression. While in the rhombohedral PZT ceramics after compression loading/unloading, the internal stresses are relatively small and generally do not reach the energy barrier for ferroelastic domain switching. Therefore, little reverse domain switching occurs in the rhombohedral PZT.

As to the morphotropic PZT, it has seven deformation modes among which six are independent, which makes it theoretically ductile in the case of deformation by ferroelastic

domain switching. The Taylor bound of the remnant strain in the morphotropic PZT after compression is not zero but equal to 0.21% which can be computed by setting the shear modulus to be infinitely large in the model. From Fig. 8, it can be estimated that only about half of the domain-switching induced strain at 400 MPa in the morphotropic PZT can be accommodated through domain orientation without generating internal stresses. Another part of switching strain (also about 0.21%) has to be constrained by neighboring grains and can generate large internal stresses, which also leads to significant reverse domain switching in the morphotropic PZT upon removing the compression. Since in experiments the domain switching induced internal stress is not that large and the internal bias field does not take effect during ferroelastic domain switching without polarization variations, the reverse domain switching is not significant for all three types of PZT ceramics as seen in Fig. 5. In another word, this model is apt to overestimate the volume fractions of reverse domain switching after compression loading, which is quite different from the case after electric poling discussed previously.

At each loading step, the volume fractions of domains in each grain can be obtained by the optimization algorithm, then the domain texture evolution process can also be reproduced by the model. Under electric loading or uni-axial compression, the domain texture is always axisymmetric about the field axis, therefore it can be described by an angular distribution function $g(\theta)\,(0 \le \theta \le \pi/2)$ of the polar axis,[27] where $g(\theta) \equiv 1$ for a random uniform distribution and the normalization condition requires $\int_0^{\pi/2} g(\theta)\sin\theta d\theta = 1$. In this work, the domain texture is described by the [001] pole figures for the tetragonal PZT, [111] pole figures for rhombohedral PZT and the cumulative pole figures of [001] and [111] axes in the morphotropic PZT ceramics. Fig. 9(a) shows the calculated domain textures of the three types of unpoled PZT ceramics subjected to maximum electric field (Fig. 7) and compression (Fig. 8), respectively. For comparison, the corresponding theoretical saturated domain textures are also presented, as seen in Fig. 9(b). It can be seen that consistent with the simulated strain curves in Figs. 7(b) and 8, the domain texture under maximum compression is closer to their saturated textures than that under maximum electric field. The simulated domain textures cannot be saturated under maximum compression of 400 MPa although in experiments, the strains seem saturated at the same stress level as seen in Fig. 5. It should be noted that for the morphotropic PZT, the theoretically saturated domain textures are dependent of the lattice deformations of both the tetragonal and the rhombohedral phases. In this work, the saturated domain textures is closer to that in the tetragonal phase because S_0^T is

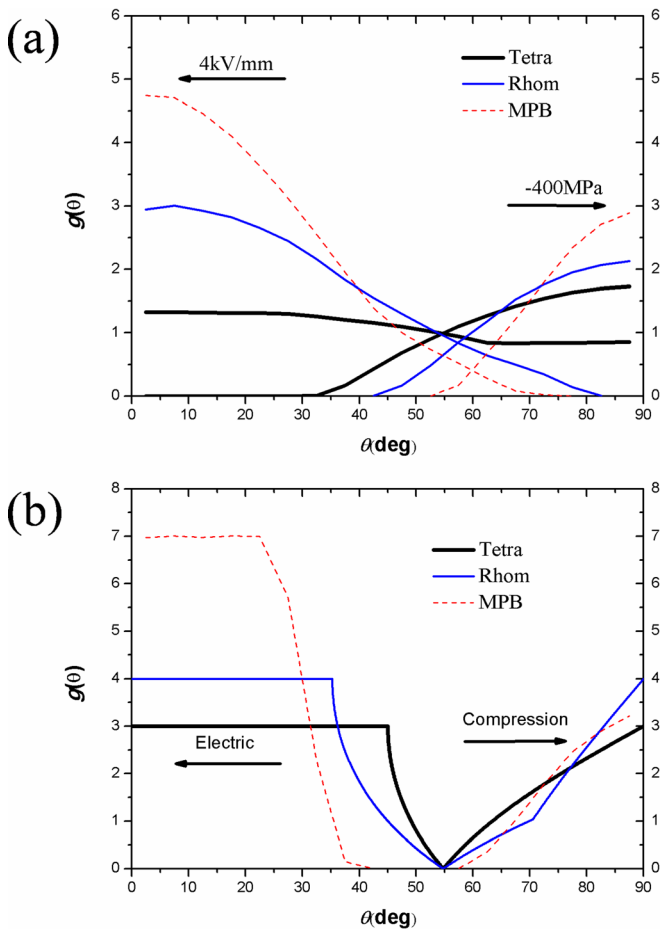

FIG. 9. The [001] pole figures in tetragonal PZT, [111] pole figures in rhombohedral PZT, and cumulative pole figures of [001] and [111] axes in morphotropic PZT ceramics subjected to complete electric poling and compression loading. (a) Simulation results; (b) theoretically saturated results.

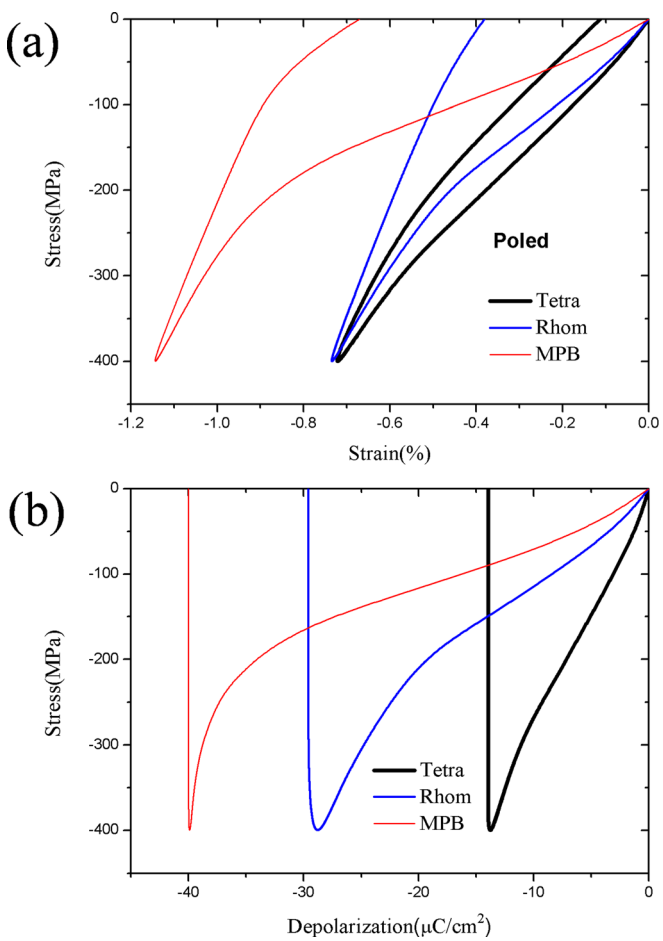

FIG. 10. The simulated (a) stress-strain curves and (b) stress-depolarization curves of the three types of poled PZT ceramics during mechanical depolarization.

larger than S_0^R then most domains turns to be tetragonal under a large compression.

The simulated depolarization curves of the three types of poled PZT ceramics are shown in Fig. 10. It can be seen that the nonlinearity of both strain and polarization in the tetragonal PZT is very small compared to that in the rhombohedral PZT and morphotropic PZT. This is easy to understand because the remnant strain of the tetragonal PZT after electric poling is very small as seen in Fig. 4(b). The maximum strain of the rhombohedral PZT is slightly larger than that of the tetragonal PZT and the maximum polarization of the former is much larger than that of the latter, which also agrees with the experiments very well. As expected, the morphotropic PZT shows the largest nonlinear strain and polarization, but both the simulated maximum strain and remnant strain are obviously larger than the experimental results in Fig. 6. This is due to the fact that as discussed earlier, in a morphotropic PZT ceramic after electric poling, the model is apt to underestimate the volume fractions of reverse domain switching and thus overestimate the switchable polarizations and strains during mechanical depolarization.

Finally, a comparison of the experimental results in Figs. 4–6 and the simulation results in Figs. 4–10 confirms that the simulations fit well with the experiments except for a few minor details. Bearing in mind that no fitting parameters were used in the model, the inherent crystal-symmetry dependent constrained domain switching in polycrystalline ferroelectrics is thought to be responsible for the observed crystal-symmetry dependent deformation in PZT ceramics.

VI. CONCLUSIONS

In summary, we fabricated three types of PZT ceramics including the tetragonal (PZT 45/55), the rhombohedral (PZT 60/40), and the morphotropic (PZT 52/48), and then conducted strain and polarization measurements during electric poling, compression loading and mechanical depolarization. Both strain and polarization of the morphotropic PZT are larger than that of the rhombohedral PZT and tetragonal PZT. The compression induced strain in unpoled tetragonal PZT is larger than that in unpoled rhombohedral PZT, while for the poled ceramics, the tendency is just on the opposite. To explore the mechanism of the observed crystal-symmetry dependent deformation in PZT ceramics, we employed a previously proposed optimization-based constrained domain switching model to simulate the experimental results. Without the use of any fitting parameters, the simulation results fit well with the experiments, which indicates the validity of the constrained domain switching model in exploring the deformation mechanism in ferroelectric ceramics.

It can be concluded that the crystal-symmetry dependent deformation mechanism in ferroelectric ceramics has been clarified in this work together with former studies.[8,9,12] The constrained ferroelastic domain switching, which is inherently crystal-symmetry dependent, is responsible for the crystal-symmetry dependent deformation in ferroelectric ceramics. The magnitude of the single-crystal deformation (S_0) strongly affects the constraint level (resisting field or stress) from the neighboring grains during ferroelastic switching, which is proportional to S_0^2 during electric loading and to S_0 during stress loading.[8,9] The Taylor's rule of plasticity is also valid for ferroelectric ceramics which indicates that the ferroelastic switching in morphotropic PZT ceramics is less constrained. Thus, the remnant strains under both electric loading and compression loading can be fairly large compared to that in the tetragonal PZT and rhombohedral PZT ceramics. Furthermore, the constrained ferroelastic domain switching is considered responsible for the observed electric-field-induced fracture in both ferroelectric single crystals[39] and ceramics.[40]

ACKNOWLEDGMENTS

F.X.L. gratefully thanks Professor Jürgen Rödel (Darmstadt University of Technology, Germany) for helpful discussions during his visit to Peking University in October 2011. F.X.L. is also grateful to Professor Nimal Rajapakse (Simon Fraser University, Canada) for his review of the manuscript and suggested revisions. Financial support from the National Natural Science Foundation of China under Grant Nos. 11002002 and 11090331 is also acknowledged.

[1]Y. Xu, *Ferroelectric Materials and Their Applications* (North-Holland Elsevier Science, Amsterdam, 1991).
[2]B. Jaffe, W. R. Cook, and H. Jaffe, *Piezoelectric Ceramics* (Academic, London/New York, 1971).
[3]S. C. Hwang, C. S. Lynch, and R. M. McMeeking, Acta Metall. Mater. **43**, 2073 (1995).
[4]M. J. Hoffmann, M. Hammer, A. Endriss, and D. C. Lupascu, Acta Mater. **49**, 1301 (2001).
[5]H. Kungl, R. Theissmann, M. Knapp, C. Baehtz, H. Fuess, S. Wagner, T. Fett, and M. J. Hoffman, Acta Mater. **55**, 1849 (2007).
[6]R. C. Rogan, "Investigation of the multi-scale constitutive behavior of ferroelectric materials using advanced diffraction techniques," Ph.D. dissertation (California Institute of Technology, 2004).
[7]A. B. Schäufele and K. H. Härdtl, J. Am. Ceram. Soc. **79**, 2637 (1996).
[8]F. X. Li and R. K. N. D. Rajapakse, Acta Mater. **55**, 6472 (2007).
[9]F. X. Li and R. K. N. D. Rajapakse, Acta Mater. **55**, 6481 (2007).
[10]D. A. Berlincourt, C. Cmolik, and H. Jaffe, Proc. IRE **48**, 220 (1960).
[11]I. Westram, H. Kungl, M. J. Hoffmann, and J. Rödel, J. Eur. Ceram. Soc. **29**, 425 (2009).
[12]J. Y. Li, R. C. Rogan, E. Üstündag, and K. Bhattacharya, Nature Mater. **4**, 776 (2005).
[13]S. C. Hwang, J. E. Huber, R. M. McMeeking, and N. A. Fleck, J. Appl. Phys. **84**, 1530 (1998).
[14]F. X. Li and D. N. Fang, Mech. Mater. **36**, 959 (2004).
[15]J. Wang, S. Q. Shi, L. Q. Chen, Y. L. Li, and T. Y. Zhang, Acta Mater. **52**, 749 (2004).
[16]B. Noheda, D. E. Cox, G. Shirane, R. Guo, B. Jones, and L. E. Cross, Phys. Rev. B **63**, 014103 (2000).
[17]D. A. Hall, A. Steuwer, B. Cherdhirunkorn, P. J. Withers, and T. Mori, J. Mech. Phys. Solids **53**, 249 (2005).
[18]F. X. Li, X. L. Zhou, and A. K. Soh, Appl. Phys. Lett. **96**, 152905 (2010).
[19]F. X. Li and A. K. Soh, Acta Mater. **58**, 2207 (2010).
[20]X. L. Zhou and F. X. Li, J. Appl. Phys. **109**, 084107 (2011).
[21]W. Tang, D. N. Fang, and J. Y. Li, J. Mech. Phys. Solids **57**, 1683 (2009).
[22]B. J. Rodriguez, C. Callahan, S. Kalinin, and R. Proksch, Nanotechnology **18**, 475504 (2007).
[23]L. B. McCusker, R. B. Von Dreele, D. E. Cox, D. Louër, and P. Scardi, J. Appl. Cryst. **32**, 36 (1999).
[24]B. Noheda, J. A. Gonzalo, L. E. Cross, R. Guo, S. E. Park, D. E. Cox, and G. Shirane, Phys. Rev. B **61**, 8687 (2000).
[25]N. Uchida and T. Ikeda, Jpn. J. Appl. Phys., Part 1 **6**, 1079 (1967).
[26]J. L. Jones, M. Hoffman, and K. J. Bowman, J. Appl. Phys. **98**, 024115 (2005).
[27]F. X. Li and R. K. N. D. Rajapakse, J. Appl. Phys. **101**, 054110 (2007).

[28]Y. W. Li, X. L. Zhou, and F. X. Li, J. Phys. D: Appl. Phys. **43**, 175501 (2010).
[29]D. C. Lupascu, *Fatigue in Ferroelectric Ceramics and Related Issues* (Springer, Berlin/New York, 2004).
[30]M. E. Lines and A. M. Glass, *Principles and Applications of Ferroelectrics and Related Materials* (Clarendon Press, Oxford, 1977).
[31]J. D. Eshelby, Proc. R. Soc. London, Ser. A **241**, 376 (1957).
[32]S. P. Han, J. Opt. Theory. Appl. **22**, 297 (1977).
[33]L. Q. Chen, Annu. Rev. Mater. Res. **32**, 113 (2002).
[34]Y. U. Wang, Y. M. Jin, and A. G. Khachaturyan, J. Appl. Phys. **92**, 1351 (2002).
[35]S. Choudhury, Y. L. Li, C. E. Krill III, and L. Q. Chen, Acta Mater. **53**, 5313 (2005).
[36]D. Schrade, R. Mueller, B. Xu, and D. Gross, Comput. Methods Appl. Mech. Eng. **196**, 4365 (2007).
[37]S. Takahashi, Ferroelectrics **41**, 143 (1982).
[38]G. I. Taylor, J. Inst. Met. **62**, 307 (1938).
[39]Y. W. Li and F. X. Li, Scr. Mater. **67**, 601 (2012).
[40]Y. W. Li and F. X. Li, Appl. Phys. Lett. **97**, 102903 (2010).